

Model calculations for an atom interacting with an intense, time-dependent electric field

L. A. Collins and A. L. Merts

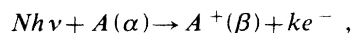
Theoretical Division (T-4), Los Alamos National Laboratory, Los Alamos, New Mexico 87544

(Received 17 November 1987)

We have performed a set of numerical calculations of the one-dimensional, time-dependent Schrödinger equation in order to study the interaction of an intense, electromagnetic field with a model atom. We approximate the atom by a local, square-well potential and the electromagnetic wave by an oscillating electric field. We investigate the multiphoton-absorption process that leads to the "above-threshold" ionization (ATI) phenomenon. We not only examine the ionization probability and electron-energy distributions within the field but also the effects of spatial and temporal boundaries that represent the finite dimensions of a laser pulse. We observe all the main features of the ATI behavior from the shifting of the peaks to their disappearance. In addition, we find differences in the positions of the peaks according to how the electron exits the field region. We also explore resonant ionization as well as Volkov wave packets and the recombination process.

I. INTRODUCTION

Recent advances in the technology of short-pulse, highly focused lasers have motivated a variety of experiments¹⁻⁷ in which atomic and molecular targets are exposed to very intense electromagnetic (EM) waves (10^{12} – 10^{17} W/cm²). Using spot sizes of a few microns and pulse durations of hundreds of femtoseconds, these experiments have achieved field strengths comparable to those that bind the atomic targets (10^{16} W/cm² \approx 0.5 a.u. of field). The exploration of this new regime has witnessed the discovery of a number of new processes, which may have profound ramifications for the study of the interaction of radiation with matter. One of the most studied of these new mechanisms is "above-threshold" ionization (ATI). The basic ionization process is described as



in which a beam of photons each with energy $h\nu$ impinges upon an atom in state α with binding energy ϵ_α and leads to an ion in state β and a free electron with energy k^2 . In the standard, weak-field ionization case, we observe a single peak in the electron-energy distribution at $k^2 = 2(h\nu - |\epsilon_\alpha|)$. However, the new bright-source lasers achieve an intensity high enough to evoke the full multiphoton process. Therefore, the electron-energy spectrum exhibits a series of peaks, separated by the photon energy $h\nu$, that correspond to the absorption of successively higher numbers of photons. In fact, cases involving the absorption of 10 to 50 photons have been recorded. In addition, the relative heights and positions of the peaks vary with the field strength. For certain characteristics of the pulse, the peaks appear to shift and even disappear as the intensity is increased. The question arises, which we shall pursue further, as to the basic nature of these phenomena.

Such findings have, of course, witnessed the revival and development of a wide variety of theoretical methods.⁸⁻³⁷ The application of standard time-

dependent (TD) perturbation theory (PT) was the most natural first choice. However, to model the full ATI structure would require very high orders of the expansion, which are usually difficult to calculate. Such an approach is therefore usually confined to weak fields for which only the lowest few orders are required. Another approach was devised by Keldysh⁹ shortly after the discovery of the laser. One prescription for obtaining his results involves the expansion of the system wave function in terms of bound target states and Volkov functions,^{9,10} which are exact solutions to the Schrödinger equation for an unperturbed electron interacting with an oscillating electric field. The evolution of the system is described in terms of a set of coupled, first-order differential equations, whose solution is the time-dependent expansion coefficients of the bound and Volkov basis. Starting with the assumption that the system remains mostly in the initial bound state, we derived a first-order form for the ionization probability that contains contributions from the principal multiphoton transitions. Higher-order contributions can be obtained by successive substitutions of the approximate solutions. Using a different gauge, Reiss¹¹ devised a similar technique based on the integral equation formulation of scattering theory. Using the homogeneous solution as an initial approximation, he obtained higher-order corrections to the wave function by repeated substitutions. Although both the Keldysh and Reiss prescriptions can be iterated to an exact solution, the forms reported by both authors and used in calculations are only valid to first order. Other formulations, using modulation theory^{13,14} and two-step schemes,¹⁶ have followed along similar lines. Despite their simplicity, these approaches predict many of the general features of the ATI process. However, many of these schemes, including those of Keldysh and Reiss, are utilized only in first order in the wave function and are of questionable validity once the system becomes appreciably ionized (probability $P > 10^{-3}$). Therefore, in order to determine the range of applicability of these approximate techniques and to investigate the regime of

more completely ionized systems, more sophisticated methods were sought.

A wide variety of more elaborate theoretical procedures have been applied to the intense field case. These have ranged from applications of Floquet theory,^{17–20} which takes advantage of the periodicity of the Hamiltonian, to the direct numerical solution of the TD Schrödinger equation.^{21–27} In many of these schemes, the δ -function model^{21,28,29} has played an important role. The basic TD formulation is greatly simplified by the replacement of the atomic potential by a δ function. The numerical approaches have ranged from the treatment of simple, one-dimensional models to elaborate TD Hartree-Fock calculations²² for hydrogen and helium. These more exact methods have not only served to test the validity of the perturbative approaches but also to probe the intricate details of the ATI process. We have presented a very brief, selective overview of the status of the experimental and theoretical endeavors on intense fields; an extensive review is available in a recent series of papers.³⁵

In this paper we have selected a simple model of the matter-radiation interaction so that we can obtain an exact numerical solution to the resulting Schrödinger equation. We represent the atomic target by a local, finite-ranged model potential in one spatial dimension. In addition, we approximate the EM wave as an oscillating electric field. Our choice of a square well serves as a transition between the δ -function potential²¹ and the long-range Coulomb form.²⁴ As we reduce the extent and increase the depth of the well, we approach the δ -function limit and can gauge the validity of this quotidian model. By widening the potential we approximate a more realistic physical target. For the basic multiphoton processes observed within the field, we obtain results in general agreement with other practitioners. In this sense, our calculations complement these earlier works. However, we also investigate the manner in which the ejected electrons exit the field, or in other words, the sensitivity of the ATI peaks to the spatial and temporal boundary conditions of the laser pulse. Since the ATI experiments show a dependence on the pulse length,^{2,4} this numerical study is particularly valuable. We have also explored the ramifications of introducing a second bound level into the potential well so that resonant ionization processes become important. In addition, we have examined the recombination process as well as Volkov wave packets. The latter quantities, which have analytical expressions for Gaussian distributions, display many of the interesting properties of the full solutions. Therefore, we conflate a diverse set of results for the multiphoton ionization within an intense EM field in order to present a unified picture of the many aspects of this process for a simple, well-defined model system.

II. THEORY

A. General time-dependent formulation

The interaction of an electromagnetic wave with an atom is described in terms of a time-dependent, three-dimensional Schrödinger equation, which must contain a

representation of the atomic target as well as the propagating radiation field. The solution to such an equation presents a most formidable task. In order to make the problem more tractable, we introduce a set of simplifying assumptions that we hope shall reduce the complexity of the solution without sacrificing the pertinent physics. We invoke the following set of simplifications: (1) we employ only one spatial dimension, (2) we represent the target by a local potential, (3) we treat the radiation field classically, and (4) we consider the electromagnetic wave to be given by an oscillating electric field.

Before delving into the mathematical formulation, we should briefly explore the consequences of these approximations. The restriction to one spatial dimension limits our models of the target system, our ability to predict continuum-electron spatial distributions, and our representation of the electromagnetic wave in that certain cross-field terms are omitted. However, in compensation, we shall be able to investigate the ionization process over a wide range of spatial and temporal variables. This flexibility allows us to properly converge the electron-energy distributions, which lie at the heart of the ATI phenomenon, and to study the manner in which the electron leaves the electric field. Our second approximation of a local, model potential to represent the atom restricts our picture of the atom-field interaction as well as of the intricacies of the atomic structure. On the other hand, the simplicity of this model will allow us to study a wide range of forms in order to ascertain the sensitivity of the various processes to the nature of the atomic potential. The third constraint to a classical representation of the radiation field is not severe. The system is now nonconservative since an unlimited number of photons can be absorbed or emitted. However, the Hamiltonian remains Hermitian, thereby preserving the norm and the continuity equation. Quantities such as ionization probabilities and electron-energy distributions are well defined. Finally, the use of only an oscillating electric field in place of the full EM wave limits our description of the general time evolution of the system, such as the passage of the front over an atom or the detailed interaction of the free electron with the field. In addition, this form completely neglects the magnetic field. However, for the intensities and frequencies employed in current lasers to study ATI, the magnetic component is very weak. On the other hand, the oscillating electric field approximation forms the basis of most intense-field approaches from the Keldysh to sophisticated numerical models. Therefore, while moderately restrictive, these approximations should not destroy the basic physical mechanisms involved in the multiphoton ionization.

The formulation of the field-atom interaction is somewhat different from that of standard scattering, being nonstationary and time dependent. We start the solution in a given initial state and follow its evolution in time and space. We effect this evolution through a solution of the following time-dependent Schrödinger equation:

$$H(x, t)\psi(x, t) = iD_t\psi(x, t), \quad (1)$$

where

$$H(x, t) = H_0(x) + H_I(x, t), \quad (2a)$$

$$H_0(x) = K(x) + V(x), \quad (2b)$$

$$K(x) = -D_{xx}/2, \quad (2c)$$

$$H_i(x, t) = xE(x, t)\cos(\omega t), \quad (2d)$$

$D_t \equiv \partial/\partial t$ and $D_{xx} \equiv \partial^2/\partial x^2$. The time-independent part H_0 contains the kinetic energy operator $K(x)$ which describes the translational motion of the continuum particle, and the local potential $V(x)$, which represents the atomic target. The interaction with the oscillating electric field is carried by the dipole-coupling term in H_i . For the one-dimensional case, the dipole representation is exact. The frequency and amplitude of the field are designated by ω and E , respectively. This corresponds to a photon energy of $h\nu$ ($\nu = \omega/2\pi$) and a period for the field of $T = 2\pi/\omega$. We have allowed for the possibility of ramping the field in space and time and have written the equation in atomic units (au) [the atomic units of length (a_0), time (τ), energy (hartrees), and electric field have the following standard equivalents: 5.29×10^{-9} cm, 2.42×10^{-17} sec = 0.0242 femtoseconds (fsec), 27.21 eV and 5.14×10^9 eV/cm]. The laser is usually characterized in terms of its intensity I , which in turn is related to the electric field [$I(\text{W/cm}^2) = 3.50 \times 10^{16} E^2$ (a.u.)]. Since we are concerned with an initial-value problem, the solution at a starting time t_0 must obey the condition

$$\psi(x, t_0) = F(x, t_0), \quad (3a)$$

with F a known function. For example, in ionization, this function F would represent the bound state of the target system, while for recombination, a wave packet corresponding to the incident particle.

For most of our studies, we shall employ a *finite-range potential* such that $V(x)$ tends to zero faster than $1/|x|$. In fact, we shall usually confine our attention to a square well of the form

$$V(x) = \begin{cases} -V_0, & |x| \leq a \\ 0, & |x| > a. \end{cases} \quad (3b)$$

The square well has the additional property of properly approaching the δ -function limit [$V \rightarrow -B\delta(x)$] as the width tends to zero and the depth to infinity while the product $2aV_0$ ($\equiv B$) remains constant. Numerous formulations have employed this δ -function potential in both one^{21,28} and three²⁹ dimensions. We therefore may be able to extend our present findings to more complicated systems by analogy with the δ -function results.

One of the observables in which we are interested is the probability of finding the electron at a given point in space and time and is given by

$$P(x, t) = \psi^*(x, t)\psi(x, t). \quad (4)$$

Since the particle must lie somewhere in the radial range at any given time, we also have

$$P(t) \equiv \int_{-\infty}^{\infty} P(x, t) dx \equiv \langle \psi | \psi \rangle = 1, \quad (5)$$

where

$$\langle \phi | \psi \rangle \equiv \int_{-\infty}^{\infty} \phi(x, t)^* \psi(x, t) dx. \quad (6a)$$

Finally, in some cases, we shall need the time average of a quantity over a period of the electric field, which we shall designate as

$$\{Q(t)\}_T^n \equiv T^{-1} \int Q(t) dt, \quad (6b)$$

where the integral extends over a period [$(n-1)T \rightarrow nT$].

B. Limiting cases

We consider several limiting cases to the general Schrödinger equation (1).

1. Potential only ($E=0$)

In this case, we recover the standard stationary-state formulation.³⁸ The time dependence can be solved exactly, and the solution takes the form

$$\psi(x, t) = \phi_\epsilon(x) \exp(-i\epsilon t), \quad (7a)$$

where

$$H_0 \phi_\epsilon(x) = \epsilon \phi_\epsilon(x), \quad (7b)$$

with ϵ the eigenenergy. For negative energies we obtain a discrete set of bound-state solutions $\{\phi_n\}$, which are normalized as

$$\langle \phi_n | \phi_m \rangle = \delta_{nm}. \quad (8a)$$

On the other hand, for positive energies, we have a continuous spectrum $\{\phi_k\}$, which exhibits the usual Dirac- δ -function normalization

$$\langle \phi_k | \phi_\kappa \rangle = \delta(k - \kappa), \quad (8b)$$

where $k^2 = 2\epsilon$.

For a *finite-range potential* in one dimension,³⁸ we have for each value of k two degenerate continuum solutions. The first represents a wave moving from left to right (ϕ_k^1), while the second designates the opposite motion (ϕ_k^2). In the asymptotic region in which the potential may be neglected, these two solutions have the following forms:

$$\phi_k^1(x) \approx \begin{cases} \exp(ikx) + R_1 \exp(-ikx), & x < 0 \\ T_1 \exp(ikx), & x > 0 \end{cases} \quad (9a)$$

$$\phi_k^2(x) \approx \begin{cases} T_2 \exp(-ikx), & x < 0 \\ \exp(-ikx) + R_2 \exp(ikx), & x > 0 \end{cases} \quad (9b)$$

$$\phi_k^2(x) \approx \begin{cases} T_2 \exp(-ikx), & x < 0 \\ \exp(-ikx) + R_2 \exp(ikx), & x > 0 \end{cases} \quad (9c)$$

$$\phi_k^2(x) \approx \begin{cases} T_2 \exp(-ikx), & x < 0 \\ \exp(-ikx) + R_2 \exp(ikx), & x > 0 \end{cases} \quad (9d)$$

where T (R) is a transmission (reflectance) coefficient, which indicates the departure of the solution from a pure plane wave. For such simple potentials as the δ -function and square well, we can determine these coefficients analytically. In the case of more complicated forms we must determine T and R from matching the numerical solutions to the above asymptotic expressions. We shall use these states to describe the ionization process.

2. Field only ($V=0$)

The solution to the time-dependent Schrödinger equation in the case of a charged particle in an oscillating electric field [$E(x,t)=E_0$, a constant] was originally derived by Volkov^{9,10} and has the form

$$\psi_v(x,t) = \chi(xt) \eta_1(t) \eta_0(t), \quad (10)$$

where

$$\chi(xt) \equiv C \exp\{i[k - \gamma_1 \sin(\omega t)]x\}, \quad (11a)$$

$$\eta_1(t) \equiv \exp[-i(\gamma_2 k^2 + \gamma_3)t], \quad (11b)$$

$$\eta_0(t) \equiv \exp\{i[-\gamma_4 k \cos(\omega t) + \gamma_5 \sin(2\omega t)]\}, \quad (11c)$$

with $C^2 = 1/(2\pi)$, $\gamma_1 = E_0/\omega$, $\gamma_2 = \frac{1}{2}$, $\gamma_3 = E_0^2/(4\omega^2)$, $\gamma_4 = \gamma_1/\omega$, and $\gamma_5 = \gamma_3/(2\omega)$. For our purposes we take the Volkov states as forming a complete set and obeying Dirac- δ -function normalization. These states will prove very useful in describing the exit of the particle from the electric field and in establishing certain properties of the electron-energy distribution.

C. Wave packets

Underlying our entire description of the time-dependent Schrödinger equation is the concept of a wave packet. We generally construct such a packet as a superposition of a complete set of known basis functions $\{\phi_k\}$ as

$$\psi(x,t) = \int_{-\infty}^{\infty} a(k,t) \phi_k(x,t) dk. \quad (12)$$

The basis is usually formed from stationary states [$\phi_k(x,t) = \chi_k(x) \exp(i\epsilon t)$] of the system although this is not a requirement so long as the set is complete. The square modulus of the quantity $a(k,t)$ is the probability of finding the system in a particular state ϕ_k at a given time t . Even though the individual continuum basis functions may obey δ -function normalization, their superposition gives rise to a total system wave function that is well behaved over all space and satisfies Eq. (5).

We now consider a few examples of such wave packets. The most common construction employs the free-particle ($V=0$, $E=0$) functions of the form

$$\phi_k(x,t) = \exp(ikx) \exp(-ik^2 t/2). \quad (13)$$

While convenient, many such functions may be required to represent the solution for propagation in a potential or field. We therefore may wish to use a stationary-state basis that contains some information about the actual system. In the case of a local potential in one dimension, we can usually obtain the bound and continuum solutions analytically or from a simple numerical integration of the time-independent Schrödinger equation [Eq. (7b)]. Due to the double degeneracy of these continuum solutions, the appropriate form for the packet is

$$\begin{aligned} \psi(x,t) = & \int_0^{\infty} a_1(k,t) \phi_k^1(x,t) dk \\ & + \int_0^{\infty} a_2(k,t) \phi_k^2(x,t) dk. \end{aligned} \quad (14)$$

The reason for this form is somewhat arcane but rests

with the fact that the Dirac- δ -function normalization condition on the ϕ^j holds only for positive k (see Ref. 38, Chap. III); the two linearly independent solutions are then required for completeness. The probability of finding the system in the state designated by k at a given time t is simply

$$P_k(t) = |a_1(k,t)|^2 + |a_2(k,t)|^2, \quad (15)$$

where

$$a_j(k) \equiv \langle \phi_k^j | \psi \rangle. \quad (16)$$

When we specifically project onto the continuum square-well solutions, we shall designate the probability as P_k^s .

As a final example, we consider a *Volkov packet* of the form

$$\psi(x,t) = \int a_v(k,t) \psi_v(x,t) dk, \quad (17)$$

where the Volkov state is given by Eq. (10). We start the solution at time $t=0$ in a particular momentum distribution,

$$a_v(k,0) = N \exp[-(k - k_0)^2 / w_k^2], \quad (18)$$

where $N^4 = 2/(\pi w_k^2)$. We have selected a Gaussian for convenience since the basic propagation properties are fairly insensitive to the form of the initial distribution. This distribution is peaked about the most probable initial velocity of the system k_0 and has a width in momentum space of w_k .

We now let the packet evolve in time according to Eq. (1) under the influence of an oscillating electric field but with no potential ($V=0$). This is the electric field analog of the free-packet propagation; both ψ and ψ_v satisfy the same time-evolution equation. Since we have not introduced any additional interactions into the time-dependent Schrödinger equation that could induce transitions among the Volkov states, the packet must remain in the same momentum distribution. We therefore have

$$P_k^v(t) \equiv |a_v(k,t)|^2 = |a_v(k,0)|^2. \quad (19)$$

We can actually solve for the time evolution of this packet analytically and obtain, for the probability density at a later time,

$$P(x,t) = c(t) \exp[-(z - k_0 t)^2 / Q(t)], \quad (20)$$

where $c(t)^2 = 1/[\pi Q(t)]$, $w_x^2 = 2/w_k^2$, $q(t) = [1 + (t^2/w_x^4)]$, $Q(t) = w_x^2 q(t)$, and $z = x - \gamma_4 \cos(\omega t)$. While complicated, this expression has a very simple interpretation. The center of the packet moves according to the form

$$x_{\text{center}} = k_0 t + (E_0/\omega^2) \cos(\omega t). \quad (21)$$

The first term represents an overall translation, which corresponds to the classical motion of a particle in free space. Superimposed on this translation is an oscillatory or "jitter" motion displayed by the second term. In addition, the packet will spread spatially according to the time dependence in the quantity $q(t)$. Although the center of the packet appears to move classically, the spread with time should alert us to the quantum-mechanical nature of the propagation. Since we are solv-

ing a complex diffusion equation, we obtain the *probability* of finding the particle in a given state k at a prescribed location. We therefore must be circumspect about classical analogies.

An interesting situation arises if we project this Volkov packet onto the free-particle stationary states of Eq. (13),

$$\psi(x, t) = \int a_f(k, t) \phi_k(x, t) dk . \quad (22a)$$

The probability $P_k^f(t)$ of finding the system in a particular stationary state is time dependent although periodic and has the simple form

$$P_k^f(t) \equiv |a_f(k, t)|^2 = |a_v(k + (E_0/\omega)\sin(\omega t), 0)|^2 , \quad (22b)$$

where a_v is given by Eq. (18). If we look *within a period*, we shall observe the center of this k -space distribution shift in position about k_0 according to

$$k_{\text{center}} = k_0 + (E_0/\omega)\sin(\omega t) . \quad (22c)$$

The expectation value of the time derivative, which in a conservative system would correspond to the total energy, has a term that grows linearly in time as $t \cos(\omega t)$. On the other hand, if we take the time average over a period of the electric field of the “kinetic energy” term [Eq. (2c)], we obtain

$$\{\langle \psi | K(x) | \psi \rangle\}_T = (k_0^2/2)[1 + (2\omega_x^2 k_0^2)^{-1}] + E_j , \quad (22d)$$

with

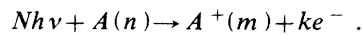
$$E_j \equiv E_0^2/(4\omega^2) . \quad (22e)$$

In the limit of an infinitely broad packet, which implies through the uncertainty principle that the momentum is precisely defined, this result approaches the classical energy of a particle moving in an oscillating electric field. The second term E_j represents the famous jitter or quiver energy. We may regard this extra term as a self-energy or in analogy with the Lamb shift, an effective mass.^{16,20} If a fixed amount of energy is supplied to the system, then part must go to the quiver motion while the remainder can result in translation. We shall return to this point in Sec. III A.

D. Ionization

1. General formulation

Multiphoton ionization is described by the following schematic reaction:



In other words, a number of photons, each with energy $h\nu$, impinge on an atom in a bound state n of energy ϵ_n producing an atomic ion in state m and a continuum electron with energy k^2 (Ry) given by

$$k^2 = 2(N\omega - |\epsilon_n|) . \quad (23)$$

We let N_0 represent the minimum number of photons needed for ionization. Even though many more photons may be absorbed, we shall characterize the ionization

process by N_0 . Therefore, an N_0 -photon ionization will have a threshold of $N_0\omega$. In the ionization process, we start the system in a bound state of the potential

$$F(x, t_0) = \phi_n(x) \exp(-i\epsilon_n t) \quad (24)$$

and evolve the solution in space and time by solving the Schrödinger equation. As time goes by, the electric field will induce transitions from this bound state into the continuum. Therefore a measure of the degree of ionization will be the amount of population in the continuum states. Since the ionization is determined from a measurement of the number of free electrons outside of the electric field, the natural representation of the continuum is in terms of the field-free stationary states [Eq. (7)]. These states would also form the proper representation if after some time we turned the field off adiabatically. In terms of these states, we have for the total ionization probability

$$P_i(t) = (2\pi)^{-1} \int |\langle \phi_k(x, t) | \psi(x, t) \rangle|^2 dk , \quad (25)$$

where the ϕ_k functions are given by Eqs. (7)–(9). If we project unto the continuum states of the square well [Eqs. (9)] then we must include both linearly independent solutions ϕ^1 and ϕ^2 , since each contains even and odd parity components. This is not a particularly convenient form to calculate since we must perform the integration over all allowed continuum states. Using the completeness of the bound and continuum basis functions, we can also write the probability as

$$P_i(t) = 1 - \sum_n |\langle \phi_n | \psi \rangle|^2 . \quad (26)$$

The sum now extends only over the discrete spectrum. For the case of a finite-range potential, which has only a small number of bound states, this form is far more tractable. In the case of an atom with a large Rydberg spectrum, the advantages are not as clear.

We can also define the ionization in terms of the probability current. Since the Hamiltonian [Eq. (1)] is Hermitian, the solution obeys the continuity equation,

$$\frac{d}{dt} \int |\psi(x, t)|^2 dx = - \int D_x j(x, t) dx , \quad (27a)$$

where the probability current is

$$j(x, t) \equiv \frac{i}{2} [\psi(D_x \psi^*) - \psi^*(D_x \psi)] \quad (27b)$$

for a range of the spatial variable from x_0 to x_1 . By integrating over time and by assuming that the ionized particle has left the vicinity of the bound wave function, we have

$$P_i(t_1) = \int j(x, t) dt , \quad (27c)$$

where the limits go from t_0 to t_1 . We have also assumed that at t_0 the system is confined to the initial state [$P_i(t_0) \equiv 0$]. If we take the proper limits, all three forms should agree.

2. Perturbation schemes

We follow the usual approach to time-dependent perturbation theory and expand the solution of Eq. (1) in

terms of a complete set of known bound $\{\phi_n\}$ and continuum $\{\chi_k\}$ states. For the case of a single-bound state ($n=b$), we have

$$\psi(x,t) = a_0(t)\phi_b(x,t) + \int a_k(t)\chi_k(x,t)dk, \quad (28a)$$

where $\phi_b(x,t) = \phi_b(x)\exp(-i\varepsilon_b t)$, and

$$H_0(x)\phi_b(x) = \varepsilon_b\phi_b(x).$$

We derive a set of coupled, first-order temporal differential equations for the coefficients $a(t)$ by substituting Eq. (28a) into Eq. (1), multiplying through by ϕ_b^* and χ_k^* , respectively, and integrating over the spatial coordinates. We begin the perturbation approach by assuming that most of the probability remains in the initial state (zeroth-order approximation)

$$a_0^{(0)}(t) \approx 1. \quad (28b)$$

We substitute this result into the coupled equations and derive a first-order approximation for the other coefficients. We obtain successively higher orders to this expansion by repeated substitutions. For the first-order corrections to be valid, the probability for the given transition must be small [$|a_k(t)|^2 \ll 1$ for all k values] in order for Eq. (28b) to hold. Technically, we can continue this iterative prescription until an exact solution is reached. In practice, since the higher-order terms become progressively more difficult to calculate, we usually confine the perturbative expansion to the lowest few terms.

The standard TD perturbation-theory form is obtained by choosing the continuum functions also to be solutions of the Hamiltonian H_0 of the unperturbed system. For N -photon ionization we have

$$P_i(t) = W_N t, \quad (29a)$$

with W_N being proportional to E^{2N} . For a single-photon process we have

$$W_1 = \pi E_0^2 |D_{mk}|^2 \rho \quad (29b)$$

for $E(x,t) = E_0 \cos(\omega t)$. The dipole matrix element is defined as

$$D_{mk} \equiv \langle \phi_m | x | \phi_k \rangle, \quad (29c)$$

with ϕ_m (ϕ_k) the bound (continuum) eigenfunction of energy ε_m ($\varepsilon = k^2/2$). The density of states (DOS) ρ depends on the choice of normalization of the continuum functions. If we choose the continuum functions to be normalized according to the relation

$$\langle b | b' \rangle = \delta(b - b')/n(b),$$

then the DOS is given by

$$\rho = n(b) db/d\varepsilon.$$

Choosing the incident plane wave to have unit amplitude as in Eq. (9), we have $b \equiv k$, $n(b) = 1/(2\pi)$, and $\rho = 1/(2\pi k)$. On the other hand, for energy normalization, we find that the DOS is unity with the variable b set to ε . We have included an additional factor of 2 in Eq. (29b) to account for the double degeneracy of the one-dimensional continuum states.

Another approach is to employ nonstationary states in the expansion. This strategy is valid provided these states form a complete set. The most common choice is the Volkov solutions, leading to the well-known Keldysh⁹ and Reiss¹¹ forms depending upon which gauge is selected. The *first-order* result is given by

$$a_k^{(1)}(t) = -i \int_{-\infty}^t \int_{-\infty}^{\infty} \phi_b^*(x,\tau) V_i(x,\tau) \chi_k(x,\tau) dx d\tau, \quad (30a)$$

where

$$V_i(x,t) = \begin{cases} xE(t) \\ iA(t)D_x/c + A(t)^2/(2c)^2 \end{cases} \quad (30b)$$

with the forms given by Keldysh and Reiss, respectively, with $E(t) = E_0 \cos(\omega t)$, and $A(t)$ the associated vector potential. For the first-order probability per unit time, we obtain in the Reiss formulation

$$W_i^{(1)} = \sum_n |\bar{\phi}_b(\kappa_n)|^2 J_n(u_n, v)^2 Q_n, \quad (30c)$$

where $\bar{\phi}_b$ is the Fourier transform of the bound-state function [$\langle \phi_k | \phi_b \rangle$, with ϕ_k given by Eq. (13)], J_n is a generalized Bessel function¹¹ of order n , $4Q_n \equiv (\kappa_n^2 - 2|\varepsilon_b|)^2$, $u_n \equiv E_0 \kappa_n / \omega^2$, $v \equiv -E_0^2 / (8\omega^3)$, and $\kappa_n^2 \equiv 2(n\omega - |\varepsilon_b| - E_j)$, with E_j given by Eq. (22e). The summation begins at the minimum number of photons needed to ionize the system, N_0 , determined by the condition that κ_n^2 is positive. We observe that even in first order this form includes an approximation to all allowed multiphoton transitions. In the limit of single-photon ($N_0 = 1$) ionization and weak electric fields, this expression for W_i will approach Eq. (29b) for standard TDPT provided we replace the length form of the dipole matrix element with the velocity and use plane waves for the continuum states. Although not restricted to weak fields, the above approach is still perturbative and depends on condition (28b) being valid. As the ionization probability approaches unity, the first-order Keldysh-Reiss formulas will also break down. We might term the electron-energy distributions obtained from the Keldysh or Reiss forms as first-order ATI (FATI) spectrum, and if all transitions are considered, we have a FATI complete.

E. Recombination

The recombination process is the reverse of photoionization, being described in the single-photon mode as

$$ke^- + A^+(m) \rightarrow A(n) + h\nu.$$

We depict this process by starting the system in a wave packet representing a particle incident upon the atom as

$$F(x, t_0) = \exp(ik_0 x) \exp[-(x - x_0)^2 / w_x^2], \quad (31a)$$

with no initial occupation in the bound states. We have employed a Gaussian distribution for the packet, centered at x_0 with a width of w_x . The leading term provides an initial velocity k_0 to the packet. As the packet passes over the atom, the oscillating electric field will induce transitions from the continuum to the bound state according to the energy condition in Eq. (23). The total probability of recombination is given by

$$P_r(t) = \sum_n |\langle \phi_n | \psi \rangle|^2, \quad (31b)$$

which is just the projection of the total system wave function on the bound states. For a tightly peaked packet and a finite-range potential, this quantity should reach a steady state once the packet has cleared the well. This particular view of recombination is a one-time process; however, the actual experimental arrangement involves a continuous beam of electrons colliding with the ion. In order to represent this arrangement we would have to form a very broad packet. For this case the probability should grow in time and be equal to the photoionization probability.

F. Ramping the electric field

The formulations of Secs. II A–II D apply for electric fields extending over all space and remaining on for all times. However, lasers produce pulses with finite spatial and temporal extents. Therefore, in order to compare with experimental findings, we must consider the effects of certain boundary conditions on the previous results. To this end, we have allowed for the departure of the electric field from its strictly oscillatory form as

$$E(x, t) = E_0 f(t) g(x), \quad (32)$$

where E_0 is the constant amplitude. In time, we have the option to linearly ramp the field up or down according to the constraint

$$f(t) = \begin{cases} (t - t_0)/(t_1 - t_0), & t < t_1 \\ 1, & t > t_1. \end{cases} \quad (33a)$$

$$(33b)$$

The field can be ramped down in time by reversing this order. We also allow for a spatial ramping in order to study the exit of the ionized particle from the field. In this case, we select the exponential form

$$g(x) = \begin{cases} 1, & x < x_1 \\ \exp[-(x - x_1)^2/(x_1 - x_2)^2], & x > x_1. \end{cases} \quad (34a)$$

$$(34b)$$

These forms of the spatial and temporal boundaries of the field roughly correspond to two distinct cases for the ionized electron exiting the laser pulse. To see this more clearly, we consider a square pulse of radial and temporal widths, x_p and t_p , respectively. We assume that the electron has a given energy k^2 , and hence a velocity v_e . Therefore, in the time that the pulse is on, the electron travels a distance $x_e = v_e t_p$. If x_e is less than x_p , then the pulse turns off in time before the electron can leave the field region. This case corresponds to the temporal ramp of Eqs. (33). For the opposite extreme ($x_e > x_p$), the electron exits the spatial region of the pulse while the field is still on. We now have conditions described by the spatial form of Eqs. (34). For convenience, we shall refer to the first case as a temporal-exit mode (TEM) and the latter as a spatial-exit mode (SEM). We shall demonstrate in Sec. III that the manner in which the ionized electron leaves the field has a profound effect on the energy distribution or ATI peaks.

G. Numerical solution

The time-dependent Schrödinger equation has the form of a complex parabolic partial differential equation (PDE). Since such equations have a long history of study, we can draw upon general, highly reliable schemes for their solution. We solve Eq. (1) numerically by a unitary form of the standard Crank-Nicholson algorithm, which is based on a finite-difference approach.³⁹ This prescription guarantees unitarity to the same order as the propagation. Since the method is implicit, at a given time we must solve for the wave function at all spatial points. This requires the solution of a set of tridiagonal linear-algebraic equations of the order of the number of spatial points. We can effect this solution either by recursion or Gaussian elimination. The spatial mesh is selected by placing between 10 and 20 points to a de Broglie wavelength ($\lambda \equiv 2\pi/k$) of the most energetic electron we wish to model ($\Delta x \approx \lambda/20$). In addition, this mesh should have a similar number of points for each oscillation of the bound function. The temporal mesh is then prescribed by the algorithm as $\Delta t = r(\Delta x)^2$. The Crank-Nicholson form has a principal truncation error on the order of $(\Delta t)^3 + \Delta t (\Delta x)^2$ and is convergent and stable for any positive value of r . We find that $r=2$ is a practical choice that gives very stable solutions over a wide range of field and potential parameters. These constraints on the step sizes determine the propinquity of the next (x, t) point. Given these optimal step sizes, we choose a spatial region $[x_i, x_f]$ large enough so that the amplitude of the wave packet at the limits is for all times very small. We find that a limit of 10^{-8} is sufficient to produce distributions and period-averaged quantities accurate to several significant figures. We start the temporal range at $t=0$ for convenience in evaluating the initial conditions although its value is completely arbitrary. With this choice of parameters, we can efficiently and accurately propagate the time-dependent Schrödinger equation.

We have tested this procedure on three cases that have analytical solutions: (1) free packet, (2) propagation in a linear potential (constant force), and (3) Volkov packet. We obtain excellent agreement for a wide range of parameters. In addition, we compare very well with the results of Goldberg, Shey, and Schwartz⁴⁰ for wave-packet scattering from a square barrier and Geltman²¹ for single-photon ionization from a δ -function potential. For each case presented in this paper we have performed several extensive tests of successively halving the spatial mesh size in order to assure convergence. In addition, since we have only a two-dimensional PDE, we need not invoke absorptive barriers to constrain the mesh. In Table I, we present typical values for the various mesh parameters for each type of problem treated.

III. RESULTS AND DISCUSSION

In this section we present the results of numerous calculations for the model established in the previous discussion. We present a sample of the many cases we have studied that best illustrates the important physical mechanisms. For most of the discussion, we shall consider a *canonical model* that employs the four approximations

TABLE I. Parameters for the solution of the TD Schrödinger equation: x_i (x_f), initial (final) value of the radial variable (a_0); Δx , radial step size; N_x , number of radial mesh points; Δt , temporal step size (a.u.).

Case	x_i	x_f	Δx	N_x	Δt
Volkov	-50	300	0.07	5000	0.02π
Ionization $N_0=1$	-200	200	0.05	8000	0.01π
Ionization $N_0=2,4$	-800	800	0.10	16 000	0.01π

listed above, in addition to considering the local potential as a square well with one bound state [Eq. (3b)]:

$$a = 0.5a_0, \quad V_0 = 0.6 \text{ hartree},$$

$$\epsilon_b = -0.130235 \text{ hartree}.$$

We have varied the well parameters and observed little sensitivity of the basic physical quantities for wells with the same ionization energy. We therefore feel that this canonical square-well model (CSWM) gives a fair representation of a broad set of calculations.

Before presenting the results of our calculations, we should briefly review the quantities defined in Sec. II, which will be of particular interest. We consider the following expressions.

(1) $P(x, t)$ is the probability of finding the particle at a given spatial and temporal point (x, t) .

(2) $P_k^\alpha(t)$ is the probability of finding the particle in a given continuum state k at a particular time t with the specific continuum projection designated by α as s , square well [Eqs. (3b) and (9)]; v , Volkov [Eq. (10)]; and f , free [Eq. (13)].

(3) $P_i(t)$ [$P_r(t)$] is the probability for ionization (recombination) at time t .

(4) $W_i(t)$ is the probability per unit time for ionization (P_i/t).

(5) N_0 is the minimum number of photons required for ionization.

We begin our discussion with a brief review of the Volkov packet.

A. Volkov packet

While not directly related to ionization, the Volkov packet illustrates several important points about the behavior of wave forms in electric fields. We consider an initial Gaussian packet as in Eq. (18) with parameters $k_0=0.5$, $x_0=0$, and $w_x=5$. This choice represents a wave function centered at $x=0$ and moving from left to right with velocity 0.5 a.u. In Fig. 1 we present the evolution of the probability density $P(x, t)$ in space and time over four periods of an electric field with $E_0=0.01$ and $\omega=0.1$. We observe as expected that the center of the packet moves according to Eq. (21) and spreads in space. We have also verified numerically that $|a_v(k, t)|^2$ remains constant about $k=0.5$ for all times. In Fig. 2 we display the square modulus of the projection of the Volkov packet onto the free-particle stationary states [Eq.

(22)] over a *single period* of the electric field. We note that this quantity shifts in position about the original distribution, as predicted by Eq. (22c). The maximum displacement of the center comes at $t=T/4$ and $3T/4$ with a magnitude of E_0/ω . This behavior of the k -space distribution during a single period is the consequence of projecting a nonstationary solution on a set of stationary states. If the field is turned off slowly in time, the excursion of the peak away from k_0 during a period becomes less pronounced. When the field becomes effectively zero, the distribution remains centered at k_0 for all later times. Many of the properties of the electron-energy distribution of the Volkov packet will manifest themselves in the ATI phenomena associated with the ionization process.

B. Ionization

1. Single photon ($N_0=1$)

We consider a single-photon ($\omega=0.2$) ionization process in the canonical model for both a weak and intense field. For the weak field ($E_0=0.003$, $I=3.15 \times 10^{11}$ W/cm²), we hope to observe the system approach the standard TDPT limit. In Fig. 3 we present the ionization probability per unit time $W_i(t)$ as a function of the number of cycles of the field ($T=10\pi$ a.u. ≈ 0.76 fsec). After

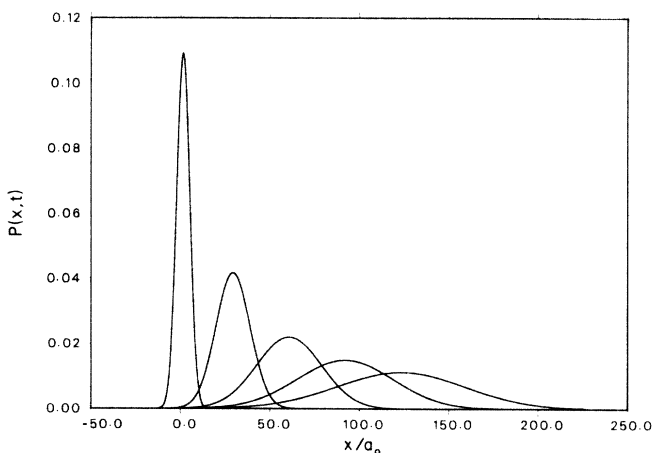


FIG. 1. Evolution in time and space of the probability density $P(x, t)$ of a Volkov wave packet with parameters $k_0=0.5$, $x_0=0$, and $w_x=5$ for an electric field of $E_0=0.01$ a.u. and $\omega=0.1$ a.u. Curves represent successive times starting at $t=0$ and extending over four periods of the field [$t=(1-4)T$].

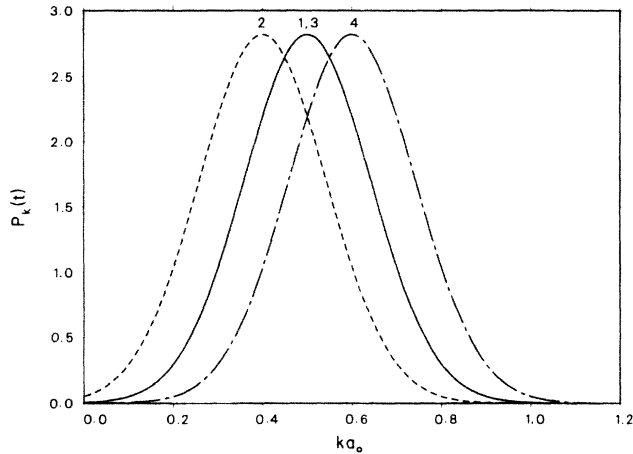


FIG. 2. Electron-energy distribution $P_k^f(t)$ as a function of wave number k and time for the Volkov packet of Fig. 1. Numbers correspond to times within a single period: 1, $t = nT$; 2, $(n + \frac{1}{4})T$; 3, $(n + \frac{1}{2})T$; 4, $(n + \frac{3}{4})T$; where $n = 3$.

an initial transitory phase, lasting less than four cycles, this quantity settles into a pattern oscillating about a constant value depicted by the dashed line. In addition, the amplitude of this oscillation damps with increasing time. This line represents a value within 2% of the standard TDPT result obtained from Eqs. (29). We display the electron-energy distribution $P_k^s(t)$ in Fig. 4 for several periods. As time passes, the distribution becomes more tightly peaked about a value corresponding to the difference between the photon and bound energies [Eq. (23)] and approaches the perturbation limit of a δ function.

We also observe several small peaks on either side of the main distribution. These arise from the manner in which the electric field is initially turned on, and not to numerical inaccuracies. To understand this behavior we

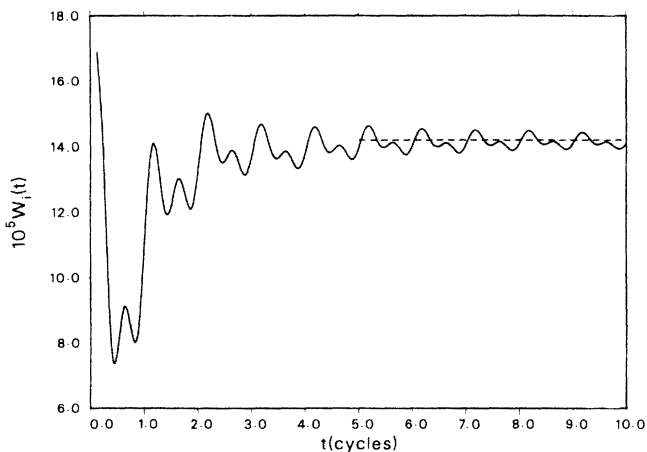


FIG. 3. Ionization probability per unit time $W_i(t)$ as a function of time [in units of periods (cycles) T of the field] for the canonical square-well model (CSWM) and $a = 0.5$, $V_0 = 0.6$, and $\epsilon_b = -0.130235$ a.u. in an oscillating electric field characterized by $E_0 = 0.003$ and $\omega = 0.2$ a.u. ($N_0 = 1$). The dashed line represents a cyclic average.

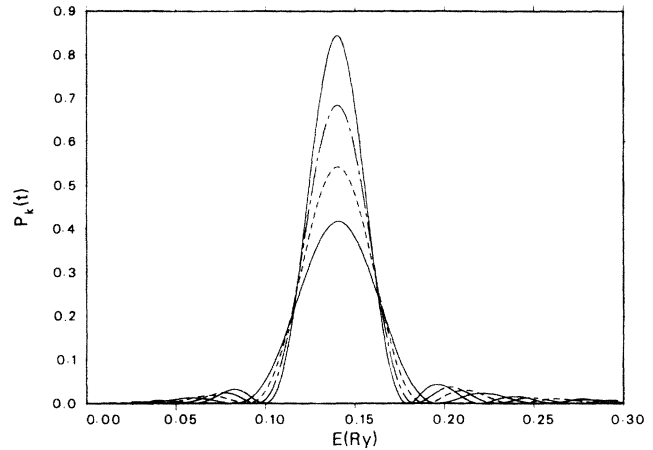


FIG. 4. Electron-energy distribution $P_k^s(t)$ as a function of energy (Rydberg) for the case described in Fig. 3. The form at four times ($t = 7, 8, 9, 10T$) is depicted.

investigate the temporal ramping of the electric field given by the function f in Eq. (32). This function describes the prescription for taking the field from zero magnitude to a final single-frequency oscillatory form [$E_0 \cos(\omega t)$]. An instantaneous turn on of the field corresponds to f being a step function, while a slower linear ramping is given by Eq. (33). Either form corresponds to a departure of the field from its single-frequency mode. In fact, if we make a Fourier analysis of the ramp function, we shall discover contributions from frequencies other than ω . These other frequencies give rise to the side peaks. However, since we are driving the system at only the frequency ω , these other components must eventually damp out once the field has reached its full oscillatory form. As time passes, the relative height of the central peak increases, and we may ignore the effects of these side components. We observe this behavior in Fig. 4 in that the central peak dominates the energy distribution for longer times. Therefore, for a weak field the numerical solutions do properly tend to the perturbation limit.

As a second example of a single-photon process we select a much stronger field [$E_0 = 0.02$ a.u., $I = 1.4 \times 10^{13}$ W/cm²]. In Fig. 5 we present the ionization probability $P_i(t)$ as a function of cycles of the field. By five cycles, the system has become over half ionized. We would therefore expect that first-order perturbation theory would not apply in this case. This expectation is borne out by the next figure (Fig. 6) of $W_i(t)$. This quantity never approaches a constant value, much less the standard perturbation result depicted by the dashed line. The system reaches saturation so rapidly that the ionization probability never settles into a long-term linear regime. In Fig. 7 we display the electron-energy distribution P_k^s at several times during a single period. As in the case of the Volkov packet, this distribution changes shape during a period. At half- and whole-period intervals, the distribution returns to a single peak, centered at an energy corresponding to the condition of Eq. (23). We observe dual peaks at quarter periods due to the projection onto the two degenerate continuum square-well solutions in Eq.

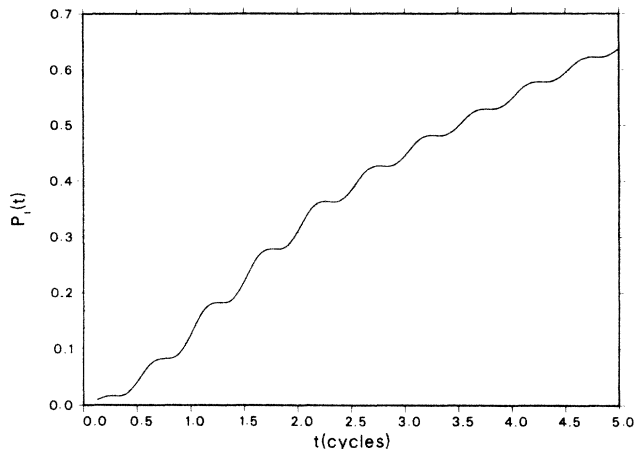


FIG. 5. Ionization probability $P_i(t)$ as a function of time for CSWM with $E_0=0.02$ and $\omega=0.2$ a.u. ($N_0=1$).

(14). As the field is slowly ramped off in time, these peaks coalesce. Their positions and relative amplitudes remain unchanged during this switch-off process. Therefore, reporting the distribution at multiples of the period, once beyond the transitory phase, corresponds to the limit of slowly turning off the field in time over many periods. We shall return to this point in more detail in Sec. III C. From the graph we obtain an energy for the center of the peak of 0.136 Ry, while Eq. (23) predicts 0.1395 Ry. The two results can be reconciled by introducing the jitter term of Eq. (22e) to give an electron energy of

$$k^2 = 2(N\omega - |\epsilon_b| - E_j). \quad (35)$$

Finally, in Fig. 8 we display the wave packet $P(x,t)$, at several periods. The distribution moves out in time as more of the bound state is ionized.

2. Multiphoton ionization

We begin with a description of ionization that requires at least two photons ($N_0=2$, $\omega=0.1$) since its basic

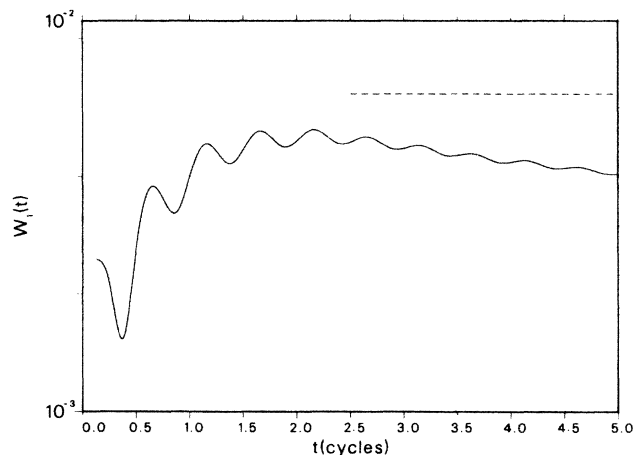


FIG. 6. Ionization probability per unit time $W_i(t)$ as a function of time for the case in Fig. 5. The dashed line represents the result of standard first-order perturbation theory.

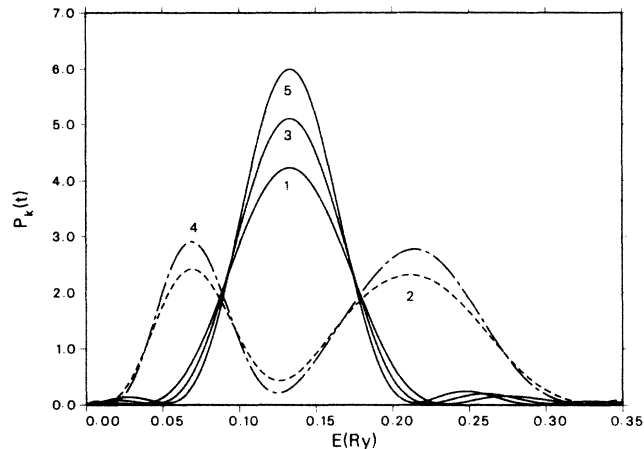


FIG. 7. Electron-energy distribution $P_k^i(t)$ as a function of energy and time for the case of Fig. 5. Numbers represent times within a single period: 1, $t=nT$; 2, $(n+\frac{1}{4})T$; 3, $(n+\frac{1}{2})T$; 4, $(n+\frac{3}{4})T$; and 5, $2nT$, where $n=4$.

features are representative of higher ionization degrees. For a weak field with $E_0=0.0075$ a.u. ($I=1.97 \times 10^{12}$ W/cm²), we obtain an ionization probability per unit time W_i that is nearly constant after a few cycles of the field. The value is within about 25% of that predicted by the Reiss formula, Eq. (30c). To investigate the high-intensity behavior, we consider a sequence of field values starting at $E_0=0.02$ a.u. ($I=1.4 \times 10^{13}$ W/cm²). Even for the lowest field value, the system becomes more than half ionized [$P_i(t) > 0.5$] after only a few periods. Therefore we are well outside the first-order perturbative regime. As an illustration we present in Table II the ionization probability at several times. In Fig. 9(a) we show the electron-energy distribution $P_k^i(t)$ for four different field strengths at $t=8T$. For the weakest field ($E_0=0.02$ a.u.), we observe three distinct ATI peaks. Their centers are separated by an energy ω and are found at positions corresponding to the condition in Eq. (35). The small os-

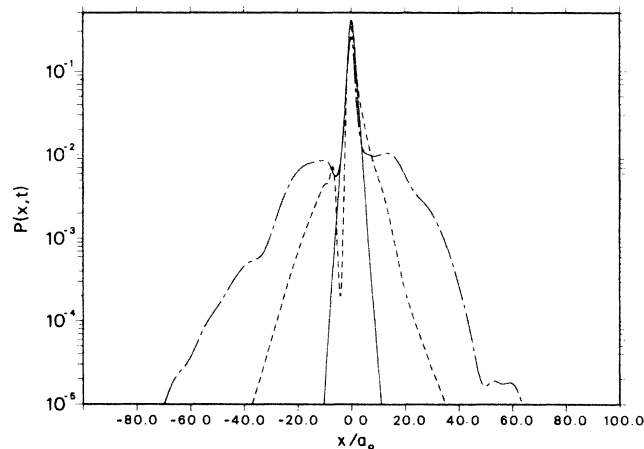


FIG. 8. Probability density, $P(x,t)$ as a function of radial coordinate x (a_0), for several times: Solid line, $t=0$; short-dashed line, $4T$; long-dashed line, $5T$.

TABLE II. Ionization probability $P_i(t)$ as a function of time and field strength (E_0) for the CSWM with $\omega=0.1$ ($N_0=2$, $T=20\pi$ a.u.) with no spatial or temporal ramps ($t_0=0$) and the mesh of Table I.

$t(T)$	E_0 (a.u.)		
	0.02	0.03	0.05
2	0.179	0.553	0.853
4	0.295	0.788	0.951
6	0.394	0.890	0.987
8	0.479	0.952	0.997
10	0.552	0.977	0.999

cillations between the principal peaks arise from the initial ramping of the electric field. They will eventually damp out at longer times as explained in Sec. II. As we increase the magnitude of the field, we observe that the peaks shift to lower energies. In addition, the amplitude of the lowest peak diminishes and practically disappears at the highest field. The explanation for this disappearance rests with the energy condition in Eq. (35). The jitter energy provides a threshold value for exciting a continuum state with translational motion. Until we have supplied an energy to the electron sufficient to excite its jitter mode, we cannot gain any net linear momentum. We should also emphasize the fact that we do not need to introduce any constant potential term to explain this suppression. In fact, the addition of such a term to the square well will simply shift the zero of energy. Since all quantities depend on energy differences, the result will be unchanged. In Table III, we present a more quantitative description of these findings. We note that a slight discrepancy still remains between the predicted results and those obtained from the graphs. This extra shift may arise from an additional effect on the bound state, although our numerical precision is not sufficient to unambiguously make this assignment. If we increase the field further, we observe the peaks to shift and vanish. In Fig. 9(b) we display the ATI spectrum for a field of 0.06 a.u. (1.38×10^{14} W/cm²). We note that the first peak has completely disappeared and that the second is highly suppressed. We also observe a whole new series of peaks at higher energies ($E > 1$ Ry). We compare this against the predictions of the first-order form of Reiss (dashed lines).^{11(a)} For this case, the Reiss form predicts an ionization probability too large by over an order of magnitude, which is not surprising given the high degree of ionization. In addition, even the relative amplitudes of the peaks are in substantial error, with the second set not predicted by the approximate form. In Fig. 10 we present the case for four-photon ($N_0=4$) ionization. The results are similar to the previous cases although exhibiting a richer spectrum.

For the multiphoton ionization process, we have observed several interesting features. First, for fields on the order of a few hundredths of an atomic unit and higher, the “atom” is completely ionized in a very few periods of the radiation field. This fact places a severe constraint on the validity of most first-order perturbative approaches. Second, we observe peaks in the electron-energy distribu-

tion separated by the photon energy ω . In addition, these ATI peaks are shifted by the jitter energy E_j according to the relation [Eq. (35)]

$$k^2 = 2[N\omega - |\varepsilon_b| - E_j].$$

Third, as the intensity increases, the lowest peaks are suppressed and eventually disappear when the photon energy is insufficient to overcome the jitter term. These particular features have all been observed experimentally and are the natural consequence of our rather simple model. We emphasize that these findings pertain to an oscillating electric field with constant amplitudes of infinite temporal and spatial extent, in other words, for the case of the ionized electrons always remaining within the field. We now turn to the effects of the spatial and temporal boundaries of the laser field on the ionization process.

C. Spatial and temporal field dependence

1. Ramping in time

We have previously discussed some of the consequences of turning on the field at some finite time t_0 . We observed additional modes at frequencies other than $N\omega$, which damped out as time passed, leaving the main ATI peaks. We are also interested in the effects on other properties of this initial switching on of the field. In Fig. 11 we present the ionization probability as a function of time for single-photon processes ($\omega=0.2$, $N_0=1$) with the canonical square-well model for $E_0=0.0075$ a.u. We investigate the effects of an instantaneous ramp as well as two linear forms. The first linear form reaches the full field E_0 at the end of two cycles [$t=2T$] while the second takes four cycles. We observe that after about ten periods all three means of ramping the field produce nearly the same results. In fact, the positions and relative magnitudes of the lowest few ATI peaks reach agreement even sooner. Thus, since we are interested in the ionization properties after a reasonable number of cycles, the exact manner of instigating the field is of little consequence.

We now investigate the effects of turning the field off after many periods. We have briefly touched on this point in Sec. II and shall illustrate it with a particular example. We choose the canonical model with a field of 0.02 a.u. and a frequency of 0.2, yielding a single-photon process. We ramp the field off in time according to Eqs. (33) from $t=6$ to $9T$. In Fig. 12 we display the electron-energy distribution at several times before, during, and after the turnoff ($t=5.25$, 8.25 , and 9.25 , respectively). We note two main features. First, the dual peaks, which arise from the projection onto the doubly degenerate continuum square-well states [Eq. (15)], coalesce to a single peak as the field dies. This single peak is centered at the half- and whole-period positions. Second, the position of the center of the peak does not change during the ramping process. Therefore, in the case in which the field is ramped off over several periods, the positions of the ATI peaks are given by Eq. (35) with the quiver energy still included. In another sense, this situation corresponds to

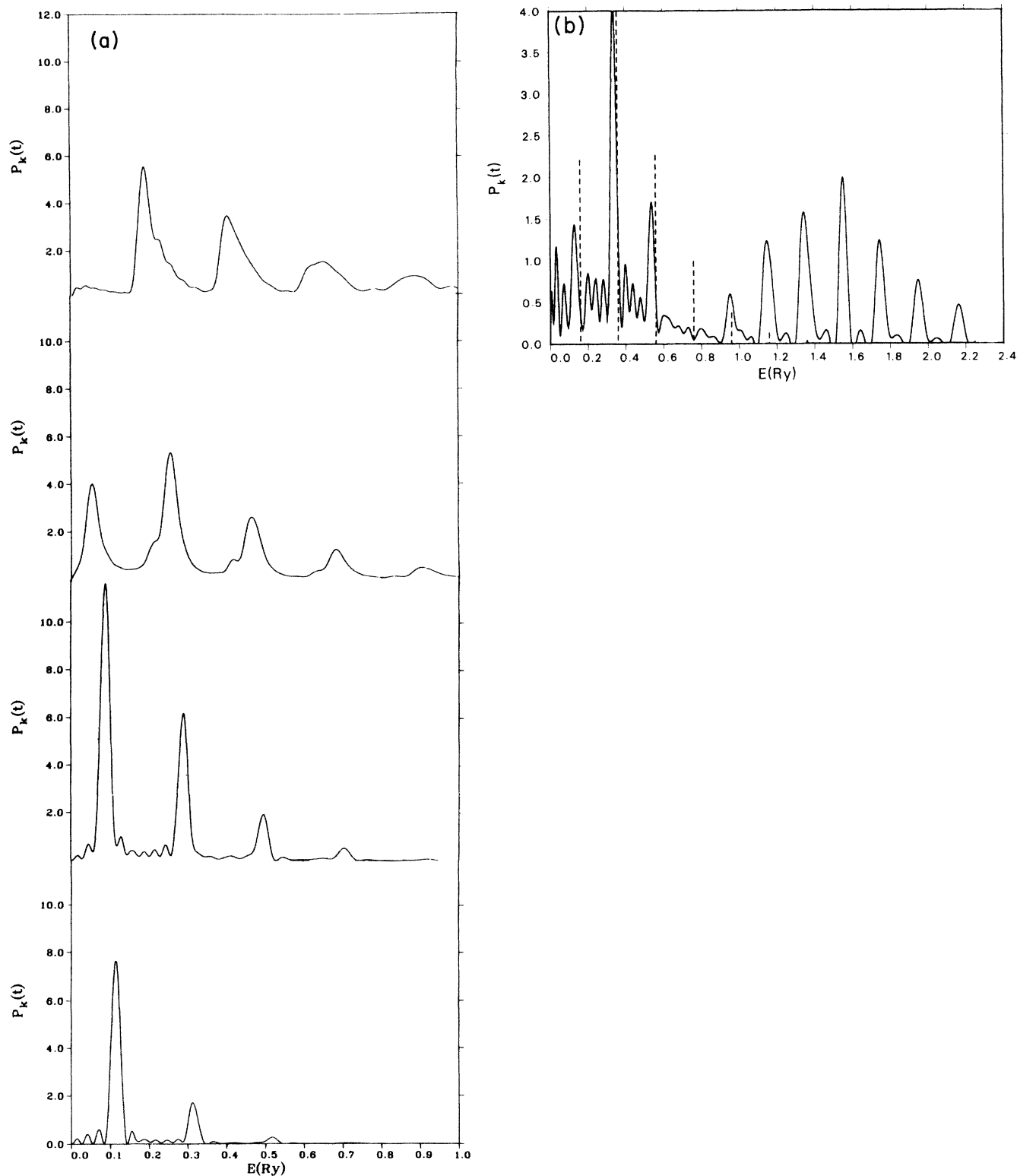


FIG. 9. (a) Electron-energy distribution $P_k^i(t)$ as a function of energy (rydbergs) for CSWM with $\omega=0.1$ a.u. ($N_0=2$) for several values of the electric field; $E_0=0.02, 0.03, 0.04,$ and 0.05 a.u., depicted from the bottom to the top of the graph, respectively. The distribution is plotted at $t=8T$. (b) Same as (a) except for $E_0=0.06$ a.u. and $t=5T$. The dashed lines represent the results of the first-order Reiss form with the second peak normalized to the CSWN result.

TABLE III. Positions of first three ATI peaks as a function of field strength (E_0) for the CSWM with $\omega=0.1$ ($N_0=2$) at $t=8T$. Entries: $k_N^2=2(N\omega - |\epsilon_b|)$; $k_j^2=k_N^2-2E_j$, where E_j is the quiver energy of Eq. (22e); k_G^2 is the calculated result read from the graph.

E_0 (a.u.)	k_N^2 (Ry)	k_j^2	k_G^2 (Ry)
0.02	0.140	0.120	0.114
0.02	0.340	0.320	0.312
0.02	0.540	0.520	0.516
0.03	0.140	0.095	0.089
0.03	0.340	0.295	0.290
0.03	0.540	0.495	0.494
0.04	0.140	0.059	0.053
0.04	0.340	0.259	0.256
0.04	0.540	0.459	0.462
0.05	0.140	0.015	
0.05	0.340	0.215	0.195
0.05	0.540	0.415	0.404

taking an “adiabatic” limit since the magnitude of the field is gradually lowered over several periods—the switching process is not abrupt. However, this effective ramp time may be quite short compared to that of the pulse. In this case, the time ramping mimics, in a rough way, the short-pulse limit in which the field switches off before the electron can extract itself and corresponds to the TEM described in Sec. II F.

2. Ramping in space

In order to investigate the effects on the ionization process of a particle exiting the field through a spatial ramp, we turn to the form given in Eq. (34). This case corresponds to an electron being able to leave the field before the pulse has had time to pass. Since the spot size of most lasers used to explore ATI is of the order of a few microns ($10^4 a_0$), we would have to propagate the solution

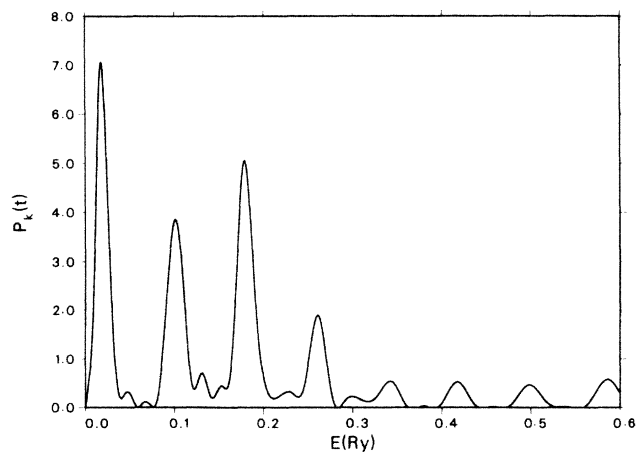


FIG. 10. Electron-energy distribution $P_k^{\xi}(t)$ as a function of energy for CSWM with $E_0=0.02$ and $\omega=0.04$ a.u. ($N_0=4$) at $t=8T$.

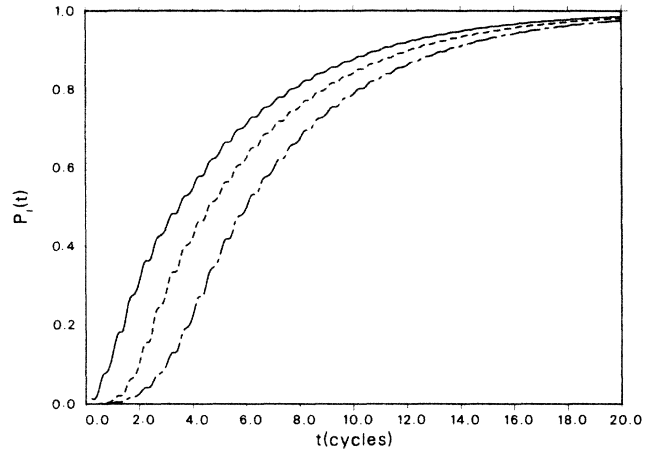


FIG. 11. Ionization probability $P_i(t)$ as a function of time (in cycles in field) for CSWM with $E_0=0.0075$ and $\omega=0.2$ a.u. ($N_0=1$). Curves represent various forms for linearly ramping on the field in time: Solid line, no ramp; short-dashed line, ramp in two periods; long-dashed line, ramp in four periods.

to extremely large distances in order to model the departure of the electron. Such spatial ranges are beyond the capability of even these simple models. However, we can still study the effect by using a Volkov packet. As time passes, the system eventually becomes completely ionized. For field strengths of a few hundredths of an a.u., complete ionization occurs within a few cycles, long before the electron can reach the edge of the pulse. The wave packet, which represents the ionized electron, moves beyond the range of the finite potential well. At this point, the projection of the total system wave function onto the Volkov states a_v becomes a constant since the potential can no longer effect transitions among the Volkov states. In other words, the packet is now propagating in a region with only an oscillating electric field in which the Volkov states form exact solutions. On the

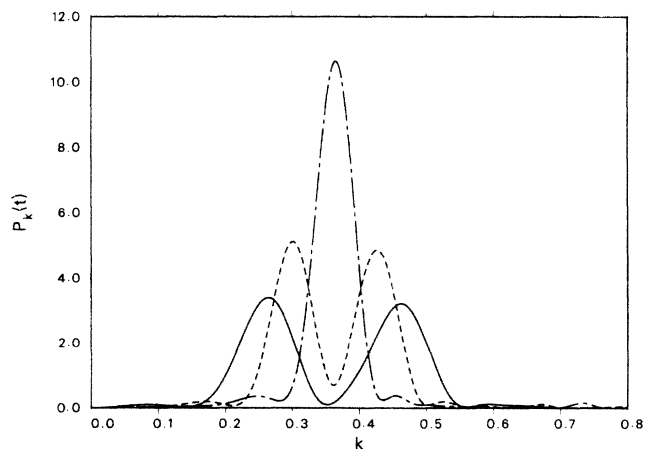


FIG. 12. Electron-energy distribution $P_k^{\xi}(t)$ as a function of the wave number for CSWM with $E_0=0.02$ and $\omega=0.2$ a.u. ($N_0=1$) for a field linearly ramped off in time between $t=6$ and $9T$. Curves correspond to different times: Solid line, $5.25T$; short-dashed line, $7.25T$; long-dashed line, $9.25T$.

other hand, the projection onto the continuum square-well states changes in time since the field continues to induce transitions. We have verified these suppositions by numerical calculations. We approximate this Volkov distribution by a Gaussian as in Eq. (18) and allow this packet to move through the spatial ramp. Since from the point at which the packet clears the well to the point at which it enters the spatial gradient the solution to the Schrödinger equation is given by a superposition of Volkov states with constant coefficients, we may start the packet fairly close to the edge of the laser beam. In order to most effectively display the effects, we have selected a Volkov packet with the following parameters:

$$k_0=1, \quad x_0=0, \quad \text{and} \quad w_x=10.$$

In this case we assume that the well is located at some large negative distance. We select the field and ramp conditions in Eqs. (32) and (34) as

$$E_0=0.20, \quad \omega=0.1, \quad x_1=100a_0, \quad x_2=300a_0.$$

In Fig. 13 we display the electron-energy distributions before and after the particle has left the field. The chief effect results from the electron gaining the jitter energy from the field. Therefore, for a spatial ramp in which the field remains on in time (SEM), the ATI peaks are not shifted by the jitter term and are positioned at the value predicted by Eq. (23), by

$$k^2=2(N\omega - |\varepsilon_b|).$$

In summary, we observe different behaviors of the electron-energy distribution according to the nature of the temporal or spatial ramp of the field. For a field slowly turned off in time over many periods (TEM), the position of the ATI peaks are the same as in the full field case and include the shift due to the quiver energy. For an electron passing through a spatial ramp (SEM), the

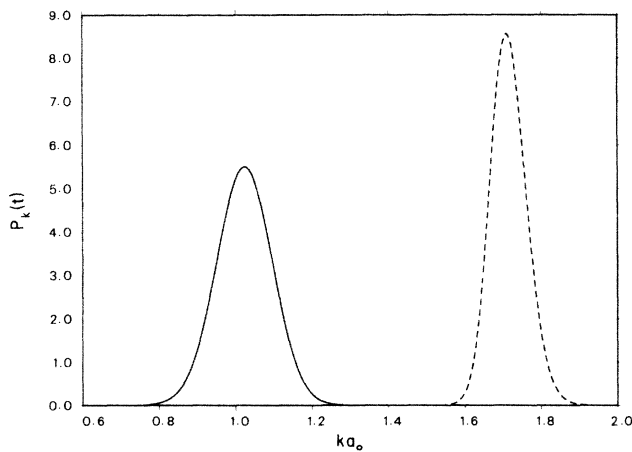


FIG. 13. Electron-energy distribution $P_k^{\pm}(t)$ as a function of wave number k for a Volkov packet ($k_0=1$, $x_0=0$, and $w_x=10$) moving through a spatially ramped electric field ($x_1=100, x_2=300a_0$) for $E_0=0.20$ and $\omega=0.1$ a.u. The solid line gives distribution at $t=0$, while the dashed line represents $t=13T$, at which time the packet is completely free of the field region.

positions shift to higher energies without a contribution from the jitter term. This difference in behavior according to how the electron leaves the field has been noted by a number of authors.^{16,31,37,41} The numerical demonstration of these effects within such a simple quantal model is most gratifying. We should be cautious about extrapolations since we have not treated the full nature of a particle interacting with an EM wave.

D. Resonant ionization

We now investigate the effects on the ionization process of placing a second bound state in the potential well. The situation is depicted in Fig. 14 in which the two levels are separated by an energy $\Delta E \equiv |\varepsilon_0 - \varepsilon_1|$. We choose the excited state to have odd parity so that dipole transitions between the two levels are allowed. We shall restrict our initial discussion to moderately weak electric fields so that we may ignore the quiver correction and the higher-order multiphoton transitions. We are particularly interested in competing ionization processes which occur when the frequency approaches the transition energy ($\Delta E \approx \omega$). The ground state can be directly ionized by a two-photon ($N_0=2$) absorption yielding a continuum electron with energy, $k_0^2=2(2\omega - |\varepsilon_0|)$. In addition, we can excite the second bound state by a resonant one-photon process and, in turn, ionize from this state by absorbing a second photon ($N_1=1$). In the latter case, the electron will be ejected with an energy, $k_1^2=2(\omega - |\varepsilon_1|)$, and the two peaks will be separated by $\Delta_s=2|\Delta E - \omega|$. Therefore we would expect the electron-energy distribution $P_k(t)$ to possess two distinct peaks at k_0^2 and k_1^2 . When the frequency of the electric field is equal to the transition energy, the two continuum electrons will leave at the same energy, and we should observe a single peak ($\Delta_s \rightarrow 0$). As we tune the frequency well away from the resonant transition energy, we should observe only the one peak arising from the ionization of the ground state since we no longer populate the excited bound level. We examine an actual model to ascertain the validity of these speculations.

We display the results in Fig. 15 for a square well ($a=2a_0$, $V_0=0.6$ a.u.; $\varepsilon_0=-0.4585$, $\varepsilon_1=-0.104$;

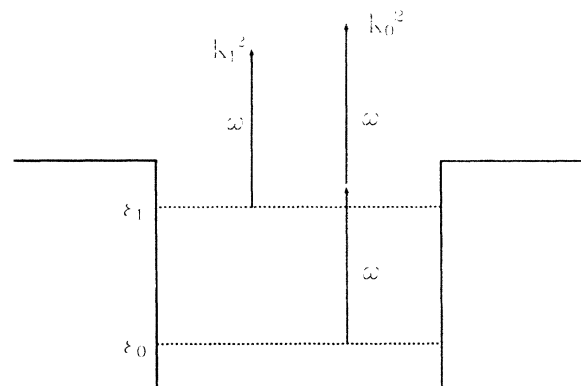


FIG. 14. Schematic representation of resonant ionization process in a square-well potential.

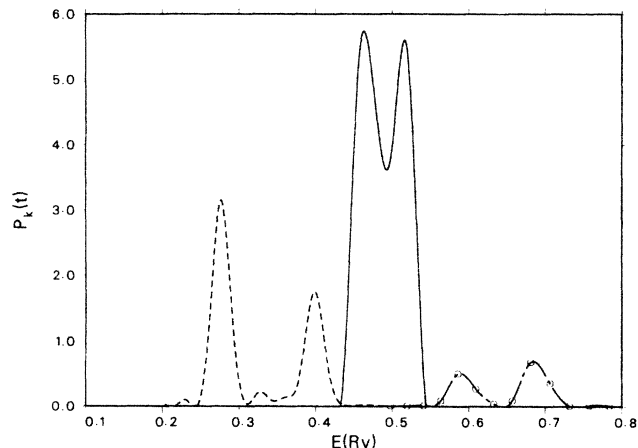


FIG. 15. Electron-energy distribution $P_k^i(t)$ as a function of electron energy and field frequency ω at $t=20T$ for $E_0=0.02$ a.u. The curves are labeled as follows: Dashed line, $\omega=0.30$; solid line, $\omega=0.35$; line with circles, $\omega=0.40$ a.u. The square well has two bound states and a width and depth of $2.0a_0$ and 0.6 a.u., respectively.

$\Delta E=0.3564$ a.u.) and for three values of the field frequency ($\omega=0.30, 0.35, 0.40$), which span the region around the resonant excitation energy ΔE . When the frequency of the electric field is smaller than the transition energy ($\omega=0.3$, dashed line), we observe two distinct peaks in the electron-energy spectrum. The lower peak corresponds to a direct two-photon ionization of the ground state, while the higher peak represents the absorption of a single photon from the excited level. The maxima of the two peaks are separated by 0.12 Ry, which is in very good agreement with the predicted value (0.11 Ry). As the frequency ($\omega=0.35$, solid line) approaches ΔE , the peaks begin to merge into a single structure. This structure again splits into two peaks as the frequency is further increased ($\omega=0.4$, circles). However, the lower peak now corresponds to the one-photon ionization of the excited state. Therefore, if we have a laser at a frequency near the transition energy of two bound states of the target atom, we might expect to observe multiple structures in the ATI peaks. In fact, Javanainen and Eberly²⁴ have reported an even richer structure for their one-dimensional Coulomb model due to resonances with the Rydberg levels. Such a repeated structure has also recently been observed in experiments⁴ on Xe. In Fig. 16 we display the probability for ionization (solid line) and for the system being in the ground (short-dashed line) or excited (long-dashed line) states for a near-resonant frequency ($\omega=0.35$). The populations of the two bound states oscillate in analogy with Rabi flopping. The overall decrease in their amplitudes comes from the steady drain of the ionization channel. Finally, we observe a pronounced enhancement in the ionization probability at the resonant frequency.

Before leaving this subject, we should make several observations. First, as the field strength E_0 is increased, we observe ATI peaks coming from absorption of larger numbers of photons. For the near-resonant case, these higher peaks also appear in groups of two with the indivi-

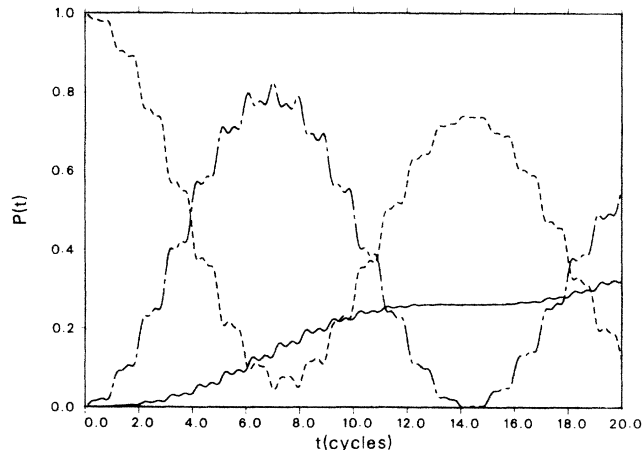


FIG. 16. Probabilities as a function of time (in periods of the field, T) for ionization (solid line), occupation of ground state (short-dashed line), and occupation of excited state (long-dashed line) for the two-state, square-well system of Fig. 15 with $E_0=0.02$ and $\omega=0.35$ a.u. ($\Delta E \approx \omega$).

dual components Δ_s apart. A given peak is, in turn, separated by ω from its counterpart in the next lower or higher group. Second, such resonant processes depend critically on the nature of the potential $V(x)$. Therefore, to properly model these structures will probably require a reasonable representation of the target atom. Third, certain two-step ionization mechanisms for ATI may be of questionable validity for this type of resonant excitation since the manner in which the electron reaches the continuum is governed by the intermediate bound state. In such a case, the process cannot be viewed as a direct ionization, followed by rearrangements amongst the continuum channels.

E. Recombination

We have also considered the recombination process. In this case, we start a Gaussian wave packet at some time t_0 according to Eq. (31a). We allow this packet to propagate in space and time according to the TD Schrödinger equation (1). At some time later, the packet will cross the finite-range potential well, and the oscillating electric field will induce transitions to the single bound state of the canonical model. In Fig. 17 we present the probability for recombination given by Eq. (31). This quantity rises as the packet experiences greater overlap with the potential well. Once the packet is completely crossed, the probability reaches a steady state. This is not quite true since the field can still produce ionization. However, since the field in this case is weak, this depletion is fairly slow. We do, however, in this wave-packet treatment observe the basic features of recombination.

IV. CONCLUSIONS

We have performed extensive numerical calculations on a simple model of an atom within an intense electromagnetic field. We confined our attention to one spa-

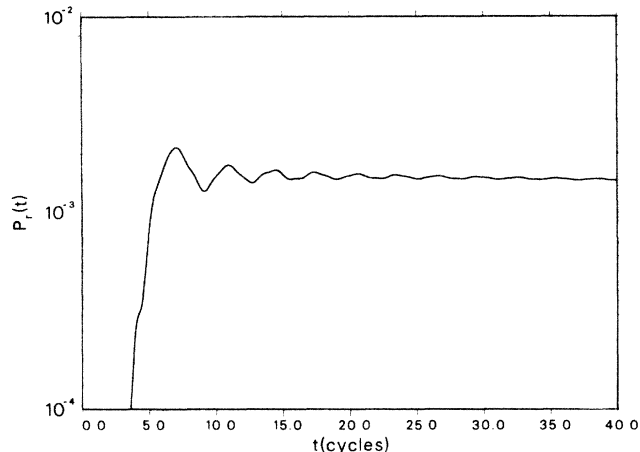


FIG. 17. Recombination probability $P_r(t)$ as a function of time for the CSWM with $E_0=0.002$, and $\omega=0.2$ a.u. for a Gaussian packet with parameters $k_0=0.375$, $x_0=-50$, and $w_x=5$ a.u.

tial dimension and to a local, finite-range representation of the atomic potential. The EM wave was approximated as a single-frequency (ω), oscillating electric field with spatial and temporal dependence [$E_0 f(t)g(x)\cos(\omega t)$] so that the general characteristics of a laser pulse could be modeled. We primarily investigated the multiphoton ionization process, leading to the ATI features in the energy distribution of the ejected electrons. In addition, we studied various mechanisms by which the electron leaves the pulse. We also explored Volkov wave packets and the recombination process.

For multiphoton ionization we observed a variety of interesting features, many of which are observed in the experimental results. First, we found that for fields of intensities above about $10^{13}\text{W}/\text{cm}^2$, the atomic system becomes significantly ionized [$P_i(t) > 0.5$] after only a few cycles of the field. This finding implies that we must be cautious about applying standard TD perturbation theory or such first-order forms as those of Keldysh and Reiss. Second, *within the field region*, we observed ATI peaks in the electron-energy distribution centered at values given by

$$k^2 = 2(N\omega - |\epsilon_b| - E_j) \equiv 2[E_b(N) - E_j] \quad (36)$$

and separated by ω . In this expression, the binding energy of the model atom is ϵ_b and the jitter or quiver energy E_j is $E_0^2/4\omega^2$. Third, as the intensity of the field is increased, the shift due to the quiver term becomes more pronounced, and the lowest peaks become suppressed. In fact, as the magnitude of the field is raised further the lowest peaks begin to disappear. This behavior is best explained by viewing the jitter energy E_j as a threshold or self-energy term. In other words, the ejected electron must first pick up the quiver energy before it can translate. For a given number of photons N , if $E_b(N)$ is less than E_j , then this mode cannot be excited, and no continuum electron appears. Therefore, within the pulse where the electric field has the form $E_0\cos(\omega t)$, the ATI peak are separated by an energy ω and start for an N

such that $E_b(N)$ exceeds E_j . However, the observed ATI spectrum also depends on the manner in which the continuum electron exits the field.

We have also made a study of the effects on the electron distribution of the spatial and temporal boundaries of the field. We allow the field to turn off in time by a linear ramp and in space by an exponential form. These ramping forms lead to very different behavior in the ATI spectrum. If the field is slowly ramped off in time over many periods, the positions of the peaks are given by the above formula, Eq. (36). This situation of a temporal ramp corresponds to the laser pulse passing over the electron before it can extract itself from the spatial region due to its radial velocity k . On the other hand, if the electron has sufficient velocity to exit the spatial realm of the beam while the field is still on, then the ATI peaks appear at values,

$$k^2 = 2(N\omega - |\epsilon_b|).$$

In other words, for a radial ramp, the electron gains back the quiver energy from the spatial gradients in the field. We should emphasize that the threshold conditions *within the field region*, which were discussed in the previous paragraph, still hold. If the difference between the N -photon and bound energies is less than the quiver term, then no ATI peak will appear. However, for those peaks with energies above the threshold, their positions will be governed by the manner of exit from the field. These effects are well documented in a recent set of experiments.^{2,4} For a pulse with a given spatial extent, as the temporal duration is shortened, the ATI peaks shift by larger and larger amounts.

Finally, we have explored the effects of introducing a second bound state of opposite parity into the potential well. When the field frequency ω approaches the transition energy ΔE , between the two bound levels, we observe groups of two AI peaks. The groups are separated in energy by ω while the individual peaks within a grouping are $\Delta_s = |\Delta E - \omega|$ apart. One peak arises from the direct N -photon ionization of the ground state. On the other hand, a second peak comes from the resonant excitation of the excited level followed by the absorption of $N-1$ photons. As we tune the frequency well away from resonance, we observe only a single peak from the direct ionization process. Such repeated ATI structures have also been observed in recent experiments.⁴

While the model we have investigated is rather simple, we still obtain most of the basic features of recent multiphoton ionization experiments for high-intensity lasers. This model allows us to systematically treat the various aspects of the ATI process and to isolate various mechanisms and deduce their relative importance.

ACKNOWLEDGMENTS

We wish to acknowledge useful discussions with Dr. K. Kulander, Dr. M. Pindzola, Dr. J. Peek, Dr. B. Schneider, Dr. D. Lynch, Dr. J. Ackerhalt, Dr. G. Schappert, and Dr. G. Csanak. This work was performed under the auspices of the U.S. Department of Energy through the Theoretical Division of the Los Alamos National Laboratory.

- ¹P. Agostini, F. Fabre, G. Mainfray, G. Petite, and N. K. Rahman, Phys. Rev. Lett. **42**, 1127 (1979); F. Yergeau, G. Petite, and P. Agostini, J. Phys. B **19**, L663 (1986).
- ²P. Agostini, J. Kupersztych, L. A. Lompre, G. Petite, and F. Yergeau, Phys. Rev. A **36**, 4111 (1987).
- ³T. J. McIlrath, P. H. Bucksbaum, R. R. Freeman, and M. Bashkamsky, Phys. Rev. A **35**, 4611 (1987); P. H. Bucksbaum, T. J. McIlrath, and L. F. Dimauro, Phys. Rev. Lett. **56**, 2590 (1986).
- ⁴R. R. Freeman, P. H. Bucksbaum, H. Milchberg, S. Darack, D. Schumacher, and M. E. Geusic, Phys. Rev. Lett. **59**, 1092 (1987).
- ⁵P. Kruit, J. Kimman, and M. van der Wiel, J. Phys. B **14**, L597 (1981); Phys. Rev. A **28**, 248 (1983).
- ⁶L. A. Lompre, A. L. Huiller, G. Mainfray, and C. Manus, J. Opt. Soc. Am. B **2**, 1906 (1985); L. A. Lompre, G. Mainfray, C. Manus, and J. Kupersztych, J. Phys. B **20**, 1009 (1987).
- ⁷T. S. Luk, T. Graber, H. Jara, U. Johann, K. Boyer, and C. H. Rhodes, J. Opt. Soc. Am. B **4**, 847 (1987); T. S. Luk, H. Pummer, K. Boyer, M. Shahidi, H. Egger, and C. K. Rhodes, Phys. Rev. Lett. **51**, 110 (1983).
- ⁸P. Lambropoulos, Comments At. Mol. Phys. **20**, 2141 (1985).
- ⁹L. V. Keldysh, Zh. Eksp. Teor. Fiz. **47**, 1945 (1964) [Sov. Phys.—JETP **20**, 1307 (1965)].
- ¹⁰D. M. Volkov, Z. Phys. **94**, 250 (1935).
- ¹¹(a) H. R. Reiss, Phys. Rev. A **22**, 1786 (1980); J. Phys. B **20**, L79 (1986); (b) F. H. M. Faisal, *ibid.* **6**, L89 (1973); B. Chen, F. H. M. Faisal, S. Jetzke, H. O. Lutz, and P. Scanzano, Phys. Rev. A **36**, 4091 (1987).
- ¹²N. M. Kroll and K. M. Watson, Phys. Rev. A **8**, 804 (1973).
- ¹³A. Dulcic, Phys. Rev. A **35**, 1675 (1987).
- ¹⁴L. Pan, B. Sundaram, and L. Armstrong, J. Opt. Soc. Am. B **4**, 756 (1987).
- ¹⁵M. Lewenstein, J. Mostowski, and M. Tippenbach, J. Phys. B **18**, L461 (1985).
- ¹⁶W. Becker, R. R. Schlicher, and M. O. Scully, J. Phys. B **19**, L785 (1986).
- ¹⁷S.-I. Chu, Adv. At. Mol. Phys. **21**, 197 (1985); S.-I. Chi and R. Y. Yin, J. Opt. Soc. Am. B **4**, 720 (1987).
- ¹⁸C. R. Holt, M. G. Raymer, and W. P. Reinhart, Phys. Rev. A **27**, 2971 (1983); S.-I. Chu and J. Copper, *ibid.* **32**, 2769 (1985).
- ¹⁹H. G. Muller and A. Tip, Phys. Rev. A **30**, 3039 (1984); H. G. Muller, A. Tip, and M. J. van der Wiel, J. Phys. B **16**, L679 (1983).
- ²⁰R. Shakeshaft, Phys. Rev. A **28**, 667 (1983); X. Tang and R. Shakeshaft, Z. Phys. D **5**, 27 (1987); Phys. Rev. A **36**, 3193 (1987).
- ²¹S. Geltman, J. Phys. B **10**, 831 (1977).
- ²²K. C. Kulander, Phys. Rev. A **35**, 445 (1987); **36**, 2726 (1987).
- ²³C. Cerjan and R. Kosloff, J. Phys. B **20**, 4441 (1987).
- ²⁴J. Javanainen and J. H. Eberly (unpublished); J. Javanainen, Q. C. Su, and J. H. Eberly, in *Atomic and Molecular Processes with Short Intense Laser Pulses*, edited by A. D. Bandrauk (Plenum, New York, in press).
- ²⁵R. V. Jensen and S. M. Susskind, in *Photon and Continuum States of Atoms and Molecules*, edited by N. K. Rahman, C. Giodotti, and M. Allegrini (Springer-Verlag, Berlin, 1987), p. 13.
- ²⁶M. S. Pindzola and C. Bottcher, J. Opt. Soc. Am. B **4**, 752 (1987).
- ²⁷A. Nauts and R. E. Wyatt, Phys. Rev. A **30**, 872 (1984); C. Leforestier and R. E. Wyatt, *ibid.* **25**, 1250 (1982).
- ²⁸A. M. Perelomov, V. S. Popov, and M. V. Terentev, Zh. Eksp. Teor. Fiz. **50**, 1393 (1966) [Sov. Phys.—JETP **23**, 924 (1966)]; **51**, 309 (1966) [**24**, 207 (1967)].
- ²⁹I. J. Berson, J. Phys. B **8**, 3078 (1975).
- ³⁰A. Szoke, J. Phys. B **18**, L427 (1985).
- ³¹E. Fiordilino and M. H. Mittleman, J. Phys. B **18**, 4425 (1985); M. H. Mittleman, *ibid.* **17**, L351 (1984).
- ³²M. Crance, J. Phys. B **17**, L355 (1984).
- ³³Z. Bialynicka-Birula and I. Bialynicka-Birula, Phys. Rev. A **33**, 1671 (1986).
- ³⁴D. Richards, J. Phys. B **20**, 2171 (1987).
- ³⁵J. Opt. Soc. Am. B **4**, 705 (1987).
- ³⁶J. Zakrzewski and K. Zyczkowski, Phys. Rev. A **36**, 4311 (1987).
- ³⁷T. W. B. Kibble, Phys. Rev. **150**, 1060 (1966).
- ³⁸A. Messiah, *Quantum Mechanics* (Wiley, New York, 1968).
- ³⁹A. R. Mitchell, *Computational Methods in Partial Differential Equations* (Wiley, New York, 1969), Chap. 2.
- ⁴⁰A. Goldberg, H. M. Shey, and J. L. Schwartz, Am. J. Phys. **35**, 177 (1967).
- ⁴¹M. H. Mittleman, *Theory of Laser-Atom Interactions* (Plenum, New York, 1982).